



Contents lists available at ScienceDirect

## Arabian Journal of Chemistry

journal homepage: [www.ksu.edu.sa](http://www.ksu.edu.sa)

# 3D printed poly(lactic acid)/poly( $\epsilon$ -caprolactone)/graphene nanocomposite scaffolds for peripheral nerve tissue engineering

Reyhane Soltani Gerdefaramarzi<sup>a</sup>, Mehdi Ebrahimian-Hosseinabadi<sup>a,\*</sup>, Mohammad Khodaei<sup>b</sup>

<sup>a</sup> Department of Biomedical Engineering, Faculty of Engineering, University of Isfahan, Isfahan 81746-73441, Iran

<sup>b</sup> Materials Engineering Group, Golpayegan College of Engineering, Isfahan University of Technology, Golpayegan 87717-67498, Iran

## ARTICLE INFO

## Keywords:

Nerve tissue engineering  
Nanocomposite scaffold  
Graphene  
Poly( $\epsilon$ -caprolactone)  
Polylactic acid  
3D printing

## ABSTRACT

This research aimed to fabricate and evaluate Poly(lactic acid)/poly( $\epsilon$ -caprolactone)/graphene (PLA/PCL/G) nanocomposite scaffolds for peripheral nerve tissue engineering. To achieve this goal, scaffolds were fabricated using the fused deposition modeling (FDM) 3D printing method with the following compositions: 50 wt% PLA-50 wt% PCL (PLA-PCL), 98.5 wt% PLA-1.5 wt% G (PLA-G), 98.5 wt% PCL-1.5 wt% G (PCL-G), and 50 wt% PLA-48.5 wt% PCL-1.5 wt% G (PLA-PCL-G). The microstructure and chemical composition of the scaffolds were characterized using SEM, XRD, and FTIR. SEM images revealed that the PLA-PCL-G scaffold exhibited a more regular and uniform morphology compared to the others, with the PLA-PCL scaffold displaying the least regularity. The porosity percentage and pore size of the scaffolds ranged from 50 % to 86 % and 300 to 500  $\mu$ m, respectively. Mechanical properties were assessed via compression testing, indicating that the elastic modulus of the PLA-PCL-G scaffold was approximately 22.36 MPa, suitable for peripheral nerve tissue applications. Electrical conductivity testing showed that PLA-PCL-G had a conductivity of about 8.2E-5 S/cm, similar to PLA-G. Biodegradability was evaluated by immersing samples in phosphate-buffered saline (PBS), revealing that PLA-PCL-G exhibited a weight loss of approximately 1.3 % and a degradation rate of 0.14 mm/day over four weeks, closely matching peripheral nerve tissue regeneration rates. MTT (3-(4,5-dimethylthiazol-2-yl)-2,5-diphenyltetrazolium bromide) assay results confirmed that PLA-PCL-G scaffolds were non-cytotoxic to PC12 cells. Overall, these findings suggest that the 50 wt% PLA-48.5 wt% PCL-1.5 wt% G scaffold holds promise for peripheral nerve tissue engineering applications.

## 1. Introduction

Statistics studies have shown that approximately 13 to 23 out of every hundred thousand people worldwide suffer from nerve injuries (Pedrosa et al., 2017). Furthermore, there are one million new cases of nerve injuries reported annually worldwide. Peripheral nerve injuries (PNIs) account for about 2 % of traumatic injuries, affecting motor function and sometimes resulting in partial or complete nerve rupture, paralysis, neuropathic pain, and sensory system damage (Wilcox et al., 2020; Yan et al., 2020; Seddighi et al., 2016; Magaz et al., 2018). Therefore, nerve injuries represent a significant human health issue, and treating these injuries is crucial. Treating nerve damage is challenging due to the complexity of tissue and its destruction mechanisms. Peripheral nervous system rehabilitation is generally more challenging than central nervous system rehabilitation due to its location in different environmental settings (Zhang et al., 2019; Lopes et al., 2022). Methods

for repairing nerve tissue are categorized into three types based on the severity of the injury: neurapraxia, axonotmesis, and neurotmesis (Bhandari, 2019). Neuropraxia is the mildest form of nerve damage, involving temporary nerve conduction blocks without disruption of axon connections or surrounding tissue, allowing for self-repair. Axonotmesis involves damage to the axon but preserves the surrounding tissue, leading to nerve stress and typically treated with medications. Neurotmesis is the most severe type, involving complete nerve rupture necessitating surgical intervention (Bhandari, 2019; Kamble et al., 2019; Costa et al., 2020). Surgical methods such as end-to-end direct suturing are straightforward but may cause tension on the nerve, potentially leading to dysfunction. Procedures using allografts and autografts have limitations; allografts face challenges such as graft rejection, while autografts may cause donor site tissue damage, neuroma formation, and compromised nerve endings and scarring (Pedrosa et al., 2017; Fornasari et al., 2020; Vijayavenkataraman et al., 2019; Howarth et al.,

\* Corresponding author.

E-mail address: [m.ebrahimian@eng.ui.ac.ir](mailto:m.ebrahimian@eng.ui.ac.ir) (M. Ebrahimian-Hosseinabadi).

<https://doi.org/10.1016/j.arabjc.2024.105927>

Received 5 April 2024; Accepted 22 July 2024

Available online 23 July 2024

1878-5352/© 2024 The Author(s). Published by Elsevier B.V. on behalf of King Saud University. This is an open access article under the CC BY-NC-ND license (<http://creativecommons.org/licenses/by-nc-nd/4.0/>).

2019). Tissue engineering combines principles from cell biology, materials science, and engineering to create tissues structurally and physiologically similar to native tissues, restoring damaged tissue function (Lee et al., 2018; Iranmanesh et al., 2022; Foroutan et al., 2021; Karimi et al., 2021). Material selection is critical; materials used in tissue engineering scaffolds must be FDA-approved and possess properties such as biodegradability and suitable elastic modulus. FDA approval limits the choice of polymers. Poly(lactic acid) (PLA), for instance, supports Schwann cells, promotes axon growth, enhances vascularization, and offers good biocompatibility, although it has drawbacks such as slow degradation rate, low impact resistance, and hydrophobicity (Lee et al., 2018; Tian et al., 2022; Vaid et al., 2021; Kasmi et al., 2021). Poly( $\epsilon$ -caprolactone) (PCL) can enhance mechanical properties of biomaterials like PLA, with higher tensile strength and elastic modulus than PLA but lower toughness and flexibility; blending PCL with PLA optimizes these properties for nerve tissue applications. Despite PCL's poor cell adhesion, combining it with PLA resolves this issue (Lee et al., 2018; Yen et al., 2019). Graphene (G) offers high flexibility, adhesion, mechanical strength compared to traditional materials, and exceptional electrical conductivity due to its unique structure, making it suitable for nerve tissue scaffolds (Novoselov et al., 2012; Fu et al., 2021; Geetha Bai et al., 2019; Zhang et al., 2020; Bei et al., 2019). Combining PLA, PCL, and graphene thus seems reasonable for fabricating nerve tissue scaffolds. Various fabrication methods exist; 3D printing addresses challenges in pore size control and scaffold network organization (An et al., 2015). Fusion Deposition Modeling (FDM), a 3D printing method utilizing extrusion and phase changes at high temperatures, offers advantages such as simplicity, cost-effectiveness, material versatility, solvent-free operation, and the ability to predict mechanical responses during cell differentiation, distinguishing it from other methods (Ceretti et al., 2017; Masood, 2014; Naghieh et al., 2016).

In this study, nanocomposite scaffolds were fabricated using FDM. Their chemical, mechanical, and biological properties were evaluated and compared, leading to the selection of the optimal composition for nerve tissue engineering scaffolds.

## 2. Materials and methods

### 2.1. Materials

Poly(lactic acid) (PLA,  $\bar{M}_w = 60000$  g/mol), poly( $\epsilon$ -caprolactone) (PCL,  $\bar{M}_w = 80000$  g/mol), MTT (3-(4, 5-di-methylthiazol-2-yl)-2, 5-diphenyltetrazolium bromide), and Trypsin-EDTA (ethylene diamine tetra-acetic acid) were supplied by Sigma-Aldrich (Germany). Graphene powder (with 95 % purity and nano-plates with a thickness of 4–20 nm) was purchased from Neutrino (Iran). Finally, PBS (Phosphate Buffer Solution), FBS (Fetal Bovine Serum), and DMEM (Dulbecco's Modified Eagle Medium) were supplied by Bioidea (Iran). All of these materials were used as received.

### 2.2. 3D printed scaffolds

For the 3D printing of scaffolds, four chemical formulations were considered: 50 wt% PLA-50 wt% PCL (PLA-PCL), 98.5 wt% PLA-1.5 wt% G (PLA-G), 98.5 wt% PCL-1.5 wt% G (PCL-G), and 50 wt% PLA-48.5 wt% PCL-1.5 wt% G (PLA-PCL-G). Initially, PLA, PCL, and G were weighed according to each scaffold's chemical formula. PLA and PCL were then dissolved in chloroform (12.50 w/v%) using a magnetic stirrer, while graphene was dispersed in chloroform in another beaker using an ultrasonic homogenizer (Ultrasonic Homogenizer, Scientz Co., China, 25 KHz, 1200 W). Ultrasonication was conducted at room temperature until a homogeneous suspension was achieved (homogenization lasted for 10 min). Subsequently, the graphene-containing suspension was gradually added to the PLA-PCL solution. The mixture was then sonicated (Parsonic 2600, Iran) for 20 min to ensure uniform dispersion of graphene nanoparticles within the PLA-PCL matrix. The resulting suspension was

poured into a flat container and left at room temperature to allow for chloroform evaporation. The composite sheets obtained were crushed and loaded into the cartridge of a 3D bioprinter (Chakad CSS1, Iran) for 3D printing, following the specifications outlined in Table 1. Similarly, PLA-PCL scaffolds (without graphene) were fabricated using a comparable process. The dimensions of the printed samples for the study were approximately 10 mm  $\times$  10 mm  $\times$  10 mm (Length  $\times$  Width  $\times$  Height).

### 2.3. Characterization of the scaffolds

Fourier transform infrared (FT-IR) spectra of the nanocomposite scaffolds were recorded using an FT/IR-6300 spectrometer (JASCO, Japan) in the range of 400–4000  $\text{cm}^{-1}$ , equipped with an attenuated total reflectance (ATR) accessory. X-ray diffraction (XRD) patterns of the scaffolds were obtained using a Cu K $\alpha$  lamp with a wavelength of 1.54 angstroms, in the range of  $10^\circ < 2\theta < 50^\circ$ , on an ADVANCE D8 X-ray diffractometer (Bruker, Germany). The morphology, 3D-printed strand diameters, porosity size, and porosity percentage of the prepared scaffolds were investigated using scanning electron microscopy (SEM) (XL30, Philips, Netherlands) at an acceleration voltage of 16 kV. The surfaces of the composites were sputter-coated with gold to eliminate surface charging effects. Additionally, the surfaces of samples used for cell culture on days 3 and 7 were observed and evaluated by SEM. Mechanical properties were evaluated according to ASTM-D3410 standards. Samples were tested in an electromechanical universal testing machine (Walter + bai, Switzerland) with a loading rate of 1 mm/min ( $n = 3$ ). Load-deformation curves were recorded, and stress-strain curves were plotted based on the obtained data. Electrical conductivity of the films was measured using a standard four-probe method with a KETHLY instrument (USA). For degradation tests, each sample was initially weighed in a dry state and then immersed in PBS solution. Samples were incubated in a digital incubator (Behdad, Iran). Weight and pH measurements were taken on days 0, 7, 14, 21, and 28. After each measurement, samples were removed from the solution, and the pH of the solution was measured using a Cyberscan pH 5500 pH meter (Eutech Instruments, USA). Removed samples were dried in the incubator and reweighed to calculate the percentage of weight loss using Equation (1) (Kumar et al., 2017):

$$\text{Weight loss (\%)} = \left( \frac{W_i - W_f}{W_i} \right) \times 100 \quad (1)$$

where  $W_i$  is the initial weight of the sample and  $W_f$  is the dry sample weight after degradation.

The degradation rate (DR) (or corrosion rate) of the composite scaffolds, from the weight loss, was calculated using equation (2) (Zakaria, 2014):

$$\text{DR} = \frac{K.W}{A.D.T} \quad (2)$$

where DR is the degradation rate (mm/year), K is a constant ( $8.76 \times 10^4$ ), T is the time of exposure (h), A is the area ( $\text{cm}^2$ ), W is the weight loss (g) and D is the density of the non-porous material ( $\text{g}/\text{cm}^3$ ).

Due to the porous nature of the scaffolds, the density of the scaffold ( $D_s$ ) was calculated using Equation (3) (Ebrahimian-Hosseinabadi et al., 2011):

**Table 1**  
3D printing parameters and values.

Parameter	Value
Nozzle diameter	400 $\mu\text{m}$
Layer thickness	300 $\mu\text{m}$
Right angle	90°
Nozzle temperature	120 °C
Print speed	5 mm/s

$$P = 1 - \frac{D_s}{D} \quad (3)$$

where  $P$  is the porosity of the scaffold, and  $D$  is the density of the non-porous material.

In Equation (2),  $D_s$  was replaced with  $D$ , and the degradation rate (DR) was calculated in mm/day. The densities of PLA, PCL, and G were considered to be 1.250 g/cm<sup>3</sup>, 1.145 g/cm<sup>3</sup>, and 2.267 g/cm<sup>3</sup>, respectively.

#### 2.4. Cell culture study

The toxicity of the samples was assessed according to the ISO 10993-5 standard. The proliferation rate and cell adhesion of PC12 cells on the scaffolds were studied and compared with control samples using the MTT assay. PC12 cells were cultured in DMEM supplemented with 10 % FBS and 1 % antibiotic-antimycotic solution (Penicillin, Streptomycin, Amphotericin, and Gentamycin) under standard cell culture conditions (37 °C, 5 % CO<sub>2</sub>, and 95 % humidity). After reaching 80–90 % confluency, the cells were detached using a 0.25 % trypsin-EDTA solution, and viable cells were counted using the trypan blue assay. Before cell seeding, the scaffolds were sterilized in 70 % ethanol for 30 min under ultraviolet light, washed twice with PBS, and incubated with DMEM for 12 h at 95 % humidity. The samples were then placed in a 24-well polystyrene culture plate (serving as a negative control). PC12 cells (Pasteur Institute of Iran, NCBI code: C153) were seeded onto the samples at a density of 10,000 cells per well and cultured in the medium at 37 °C, 5 % CO<sub>2</sub>, and 95 % humidity. The cell culture control sample was maintained in a normal environment without any scaffold samples. The medium was replaced every other day. The proliferation rate was investigated on days 1, 3, and 7 after cell seeding in the 24-well plate. PC12 cells were washed with PBS to remove nonviable cells and exposed to a fresh medium containing 10 % MTT dye solution (5 mg/mL) to form formazan. After 4 h of incubation at 37 °C in 5 % CO<sub>2</sub>, the scaffolds were removed from the MTT solution, and the formazan was dissolved in a sterile DMSO solution. The absorbance of each well was measured at 490 nm using an ELISA reader (Bio-Rad, USA). Each group was measured in triplicate. Cell viability was calculated using Equation (4) (Kamiloglu Beştepe et al., 2020):

$$\text{Relative cell viability (\%)} = \left( \frac{A_{\text{sample}} - A_b}{A_c - A_b} \right) \times 100 \quad (4)$$

where  $A_{\text{sample}}$  is the absorption of the desired sample,  $A_c$  is the absorption of the control sample, and  $A_b$  is the blank absorption.

In addition, cell attachment was investigated using PC12 cells. SEM images were taken to evaluate the morphologies of the cells and the

surface of the scaffolds on day 3. Before imaging, the cells were fixed to the surface using a glutaraldehyde solution.

#### 2.5. Statistical and image analysis

All experimental data were expressed as mean  $\pm$  standard deviation (SD). Statistical analysis was carried out using single-factor analysis of variance (ANOVA). A value of  $P < 0.05$  was considered statistically significant. Porosity percentage was measured using MATLAB version 8 (2013), and strand diameters were measured using ImageJ version 44.1 software.

### 3. Results and discussion

XRD patterns (Fig. 1) of the PCL-PLA-G, PLA-G, PCL-G, and PCL-PLA scaffolds characterized three types of peaks corresponding to PLA, PCL, and graphene in the desired range. By comparing the XRD patterns of PLA-G, PCL-G, and PCL-PLA-G, a common peak in the  $2\theta$  range between 25 and 30 degrees can be identified, which is related to the presence of graphene. The intensity of this peak is lower than the others, indicating a low amount of graphene (1.5 %). Additionally, there are two peaks in the  $2\theta$  intervals between 20 and 25 degrees in the PCL-PLA, PCL-G, and PCL-PLA-G spectra, indicating the presence of PCL in the final samples. Another two peaks in the  $2\theta$  range between 15 and 20 degrees in the PCL-PLA, PLA-G, and PCL-PLA-G samples indicate the presence of PLA in these compounds.

The FTIR patterns (Fig. 2) of the PLA-PCL-G, PLA-G, PCL-G, and PLA-PCL scaffolds revealed that all functional groups related to PLA, PCL, and nano-graphene are present. Specifically, the intense bands at 2995 and 2944 cm<sup>-1</sup> in PLA, and 2946 and 2867 cm<sup>-1</sup> in PCL are related to C–H bonds. Additionally, the intense bands at 1755 cm<sup>-1</sup> in PLA and 1727 cm<sup>-1</sup> in PCL, which are related to C=O bonds, were observed in the samples. The intense band at 1729 cm<sup>-1</sup>, which is due to the stretching of the carbonyl group and is related to the C=O functional group, intensifies with the increasing percentage of PCL. Therefore, it is absent in the PLA-G sample and has the highest intensity in the PCL-G sample. The intense band at 1190 cm<sup>-1</sup>, which is due to C–O–C bonds, and the intense band at 1241 cm<sup>-1</sup>, due to C–O and C–C bonds, indicate the presence of PCL in the PCL-G, PLA-PCL-G, and PLA-PCL samples.

The SEM images (Fig. 3a to 3d) confirmed that the structure and arrangement of samples containing graphene nanoparticles (Fig. 3a to 3c) are more regular compared to the PLA-PCL sample (Fig. 3d). Upon comparing Fig. 3a, Fig. 3b, and Fig. 3c, it appears that the interaction of PCL and PLA with graphene resulted in a more regular structure. The pore size of the PCL-PLA-G scaffolds was approximately 500  $\mu\text{m}$  (Table 2). Additionally, the results indicated a significant reduction in

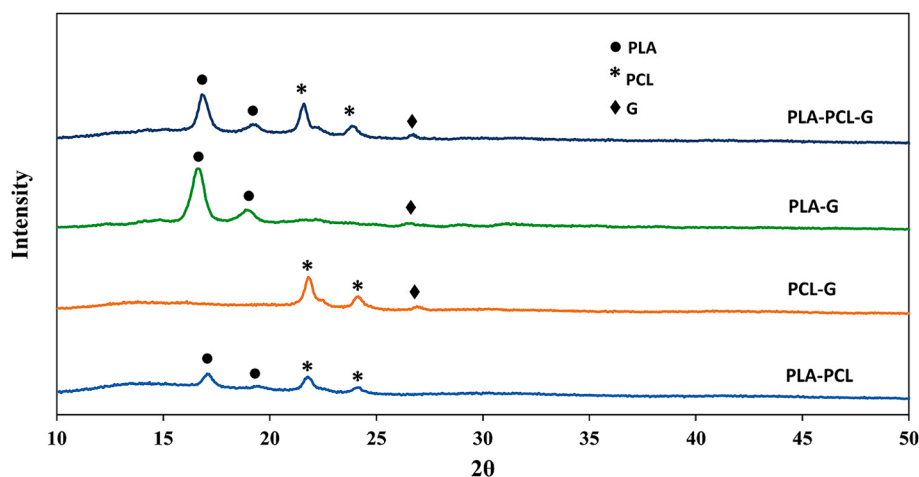


Fig. 1. XRD patterns of the PLA-PCL-G, PLA-G, PCL-G, and PLA-PCL scaffolds.

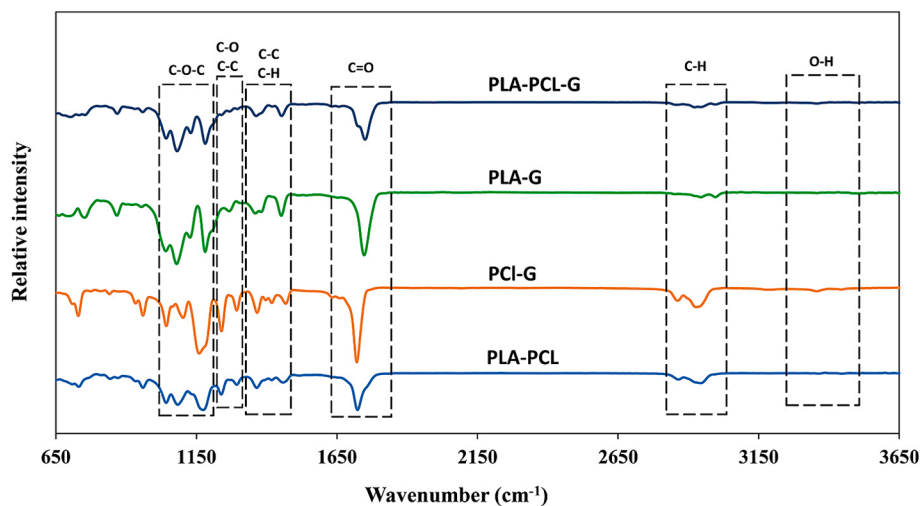


Fig. 2. FTIR spectra of the PLA-PCL-G, PLA-G, PCL-G, and PLA-PCL scaffolds.

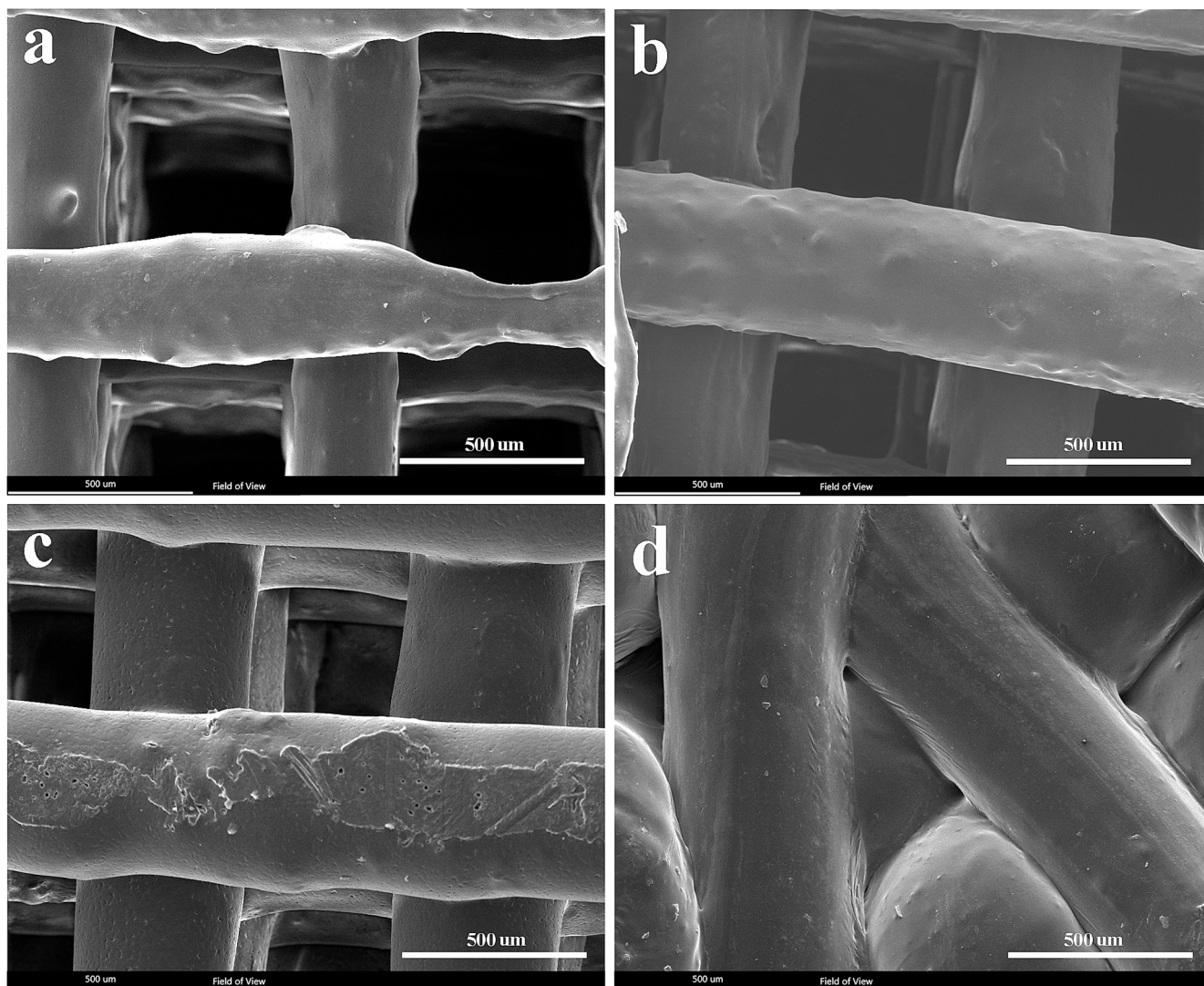


Fig. 3. SEM images of the scaffolds. PLA-PCL-G, b) PLA-G, c) PCL-G, and d) PLA-PCL.

**Table 2**

The average porosity size, porosity percentage, and strand diameters of the composite scaffolds.

Scaffold	porosity size ( $\mu\text{m}$ )	Porosity (%)	strand diameters ( $\mu\text{m}$ )
PLA-PCL-G	500 $\pm$ 13.11	86.02 $\pm$ 2.31	251 $\pm$ 17
PLA-G	407 $\pm$ 25.24	72.86 $\pm$ 5.33	435 $\pm$ 119
PCL-G	376 $\pm$ 25.51	77.52 $\pm$ 7.29	416 $\pm$ 180
PLA-PCL	300 $\pm$ 33.51	50.04 $\pm$ 8.84	601 $\pm$ 35

strand diameter with the addition of graphene to PLA-PCL; the diameter of PLA-PCL-G strands is approximately 250  $\mu\text{m}$ . The presence of graphene decreased strand diameter, which can be attributed to challenges in achieving uniform dispersion of graphene and affecting material flow during FDM printing. Graphene's hydrophobic nature and poor inter-layer adhesion can lead to insufficient bonding between layers, potentially causing delamination and thinner strands (Wu et al., 2023; Firoozabadi et al., 2022). Furthermore, the addition of graphene to PLA, PCL, and PLA-PCL composites can alter the thermal conductivity of the material, affecting extrusion behavior even at consistent printing temperatures across all samples. Increased thermal conductivity due to graphene can accelerate cooling at the nozzle, potentially influencing the consistency of strand width during extrusion (Wang et al., 2019; Lei et al., 2022). In contrast, Fig. 3d suggests that the absence of graphene results in more irregularities (pore sizes of approximately 300  $\mu\text{m}$  and a porosity level of about 50 %) and thicker strands (around 600  $\mu\text{m}$ ). This scaffold may affect cell behavior unfavorably compared to other scaffolds (Khajehmohammadi et al., 2023; Zhang et al., 2022).

Fig. 4 shows the weight loss of the samples over 28 days. All samples exhibited an upward degradation trend; the PCL-PLA-G sample showed the highest degradation with a weight loss of approximately 1.3 %, while the PCL-G sample had the lowest degradation at about 0.2 %. The primary cause of degradation for PLA and PCL polymers is the hydrolysis of ester groups, influenced by laboratory conditions such as temperature (Seyedsalehi et al., 2020; Wu et al., 1998; Shamsah et al., 2020). Moreover, the molecular weight of polymers affects this phenomenon; the lower molecular weight of PLA compared to PCL used in this study resulted in higher degradation of PLA than PCL. While molecular weight can influence degradation rates to some extent, other factors such as chemical structure, environmental conditions (e.g., temperature, humidity), and the presence of additives or reinforcements (like graphene) play crucial roles (Sazali et al., 2020; Kim et al., 2019). Fillers such as graphene can alter polymer degradation kinetics by affecting surface

interactions and water absorption characteristics. Additionally, the presence of graphene reduced the thickness of the strands, thereby increasing the surface area available for degradation per unit volume. This can also lead to increased release of graphene particles into the medium during degradation.

When investigating the degradation behavior of scaffolds for neurons, it should be considered that the scaffold degradation rate corresponds to the rate of neuronal regeneration (Papageorgiou et al., 2017; Sensharma et al., 2017). Researchers (Sulaiman and Gordon, 2013; JAWEED, M., 1994) have reported that the regeneration rate of peripheral nerve tissue is approximately 0.2–1 mm/day. According to Table 3, the degradation rate of PLA-PCL-G is significantly higher compared to the others, with a value of 0.144 mm/day, which closely matches the regeneration rate of peripheral nerve tissue. Therefore, the degradation behavior of PCL-PLA-G appears to be favorable for peripheral nerve tissue engineering.

According to Fig. 5, all samples exhibited an alkaline pH during the first week of degradation, attributed to the breakdown of L-glutamine and accumulation of ammonia in the degradation medium (Chiesa et al., 2020). By the second week, pH levels became slightly more acidic compared to the first week, likely influenced by the higher degradation rates of polymers. In the third week, except for the PLA-G sample, pH levels increased again, and by the fourth week, pH values remained higher than in the previous week but lower than initial values. It appears that alkaline pH values in the solutions correlate indirectly with the rate of polymeric degradation. The alkaline environment during degradation provides favorable biological conditions for growth and cell proliferation, suggesting these compositions do not exhibit cytotoxic effects.

As evident in Fig. 6, among the four scaffolds with PLA-PCL, PCL-G, PLA-G, and PLA-PCL-G compositions, the elastic modulus of PLA-G and PLA-PCL scaffolds has significantly the highest and lowest values, respectively. It is clear that graphene has increased the modulus of

**Table 3**

The degradation rate (DR) of composite scaffolds was calculated using equations (2) and (3).

Scaffold	D ( $\text{g}/\text{cm}^3$ )	D <sub>s</sub> ( $\text{g}/\text{cm}^3$ )	DR (mm/day)
PLA-PCL-G	1.205	0.168	0.144
PLA-G	1.258	0.342	0.019
PCL-G	1.154	0.259	0.021
PLA-PCL	1.195	0.597	0.035

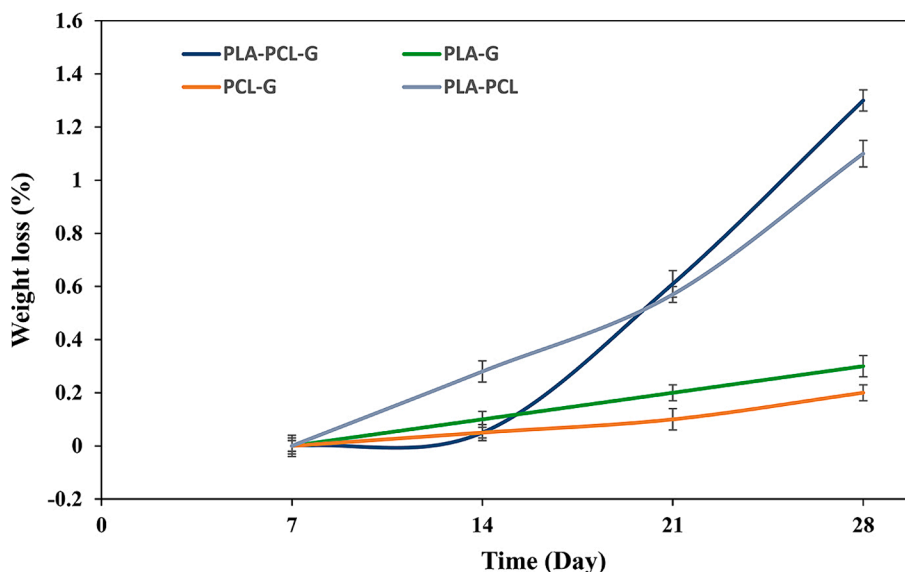


Fig. 4. The weight loss during the 28-day degradation period.

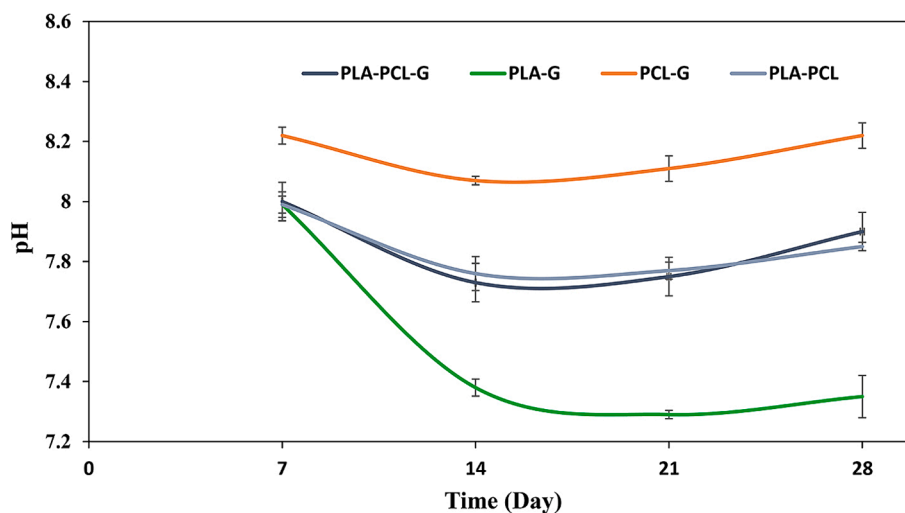


Fig. 5. The pH of simulated body fluid (SBF) during the 28-day degradation period.

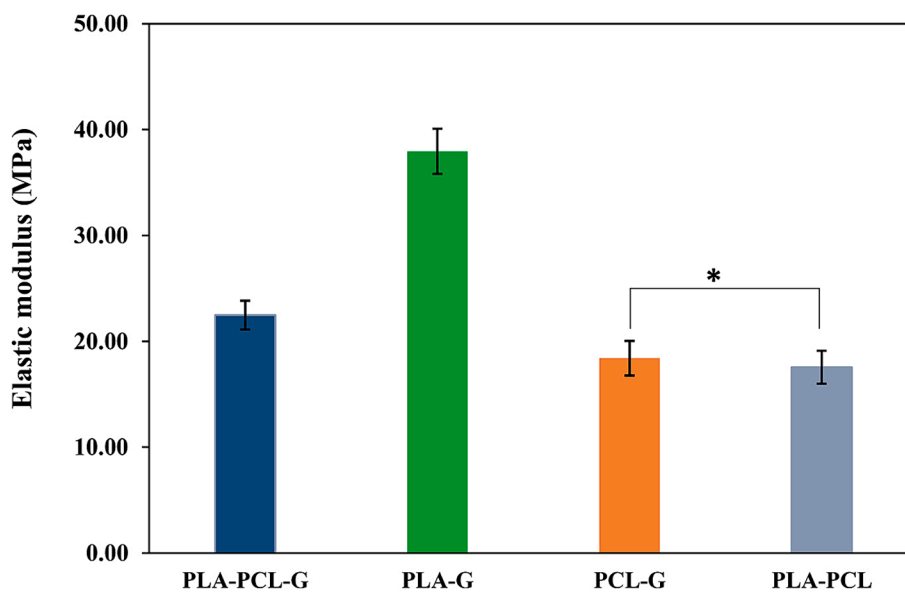


Fig. 6. Elastic modulus of the scaffolds with various compositions (\*  $P > 0.05$ ).

elasticity overall. Comparing the two samples, PCL-G and PLA-G, it is concluded that PLA significantly enhances mechanical properties compared to PCL, as evidenced by PLA's higher modulus (approximately 1133 MPa as a bulk material) compared to PCL (approximately 430 MPa as a bulk material) (Chiesa et al., 2020; Bayer, 2017). This value is approximately three times higher for PLA compared to PCL. On the other hand, comparing PCL-PLA and PCL-G, these two samples do not show significant differences from each other. Therefore, it seems that adding 50 % PLA to PCL is nearly equivalent to adding 1.5 % graphene. This evidence suggests that the effect of graphene on mechanical properties is greater than that of PLA (Bayer, 2017; Eshraghi and Das, 2010; Hasheminejad and Montazeri, 2020; Ramazani and Karimi, 2016). Finally, since the modulus of elasticity of peripheral nerves is very low (0.5–13 MPa), all samples except the PLA-G sample appear more suitable for the intended application (Mankavi et al., 2023). Closer mechanical properties of scaffolds to tissue facilitate the cell growth and proliferation process.

Electric conductivity is crucial in peripheral nerve tissue engineering for various reasons. Firstly, it facilitates communication within the body by transmitting electrical impulses essential for movement and bodily

functions. Engineered tissues mimicking nerve conductivity integrate better with the nervous system, aiding communication with surrounding nerves. Secondly, it enhances regeneration; electrical stimulation promotes nerve cell growth, crucial for restoring function after injury. Electrically conductive tissues provide an optimal environment for regeneration. Moreover, they improve functionality by enabling signal transmission across injury sites, enhancing motor control and sensory perception. Lastly, bioelectronic interfaces benefit from nerve tissue conductivity, enabling communication with external devices like prosthetics or sensors (Park et al., 2020; Sun et al., 2023; Masarra et al., 2022). Fig. 7 illustrates that samples containing graphene particles have significantly higher conductivity compared to samples without graphene. Graphene particles are conductive, and this property increases the electrical conductivity of the scaffolds containing graphene. Therefore, PLA-PCL showed the minimum electrical conductivity. There are no significant differences among the three samples containing graphene particles (PLA-PCL-G, PLA-G, and PCL-G). However, the PLA-PCL-G and PLA-G samples showed higher values, which can be attributed to better dispersion and interaction of graphene particles within the PLA matrix or the PLA-PCL blend, leading to more efficient conductive pathways.

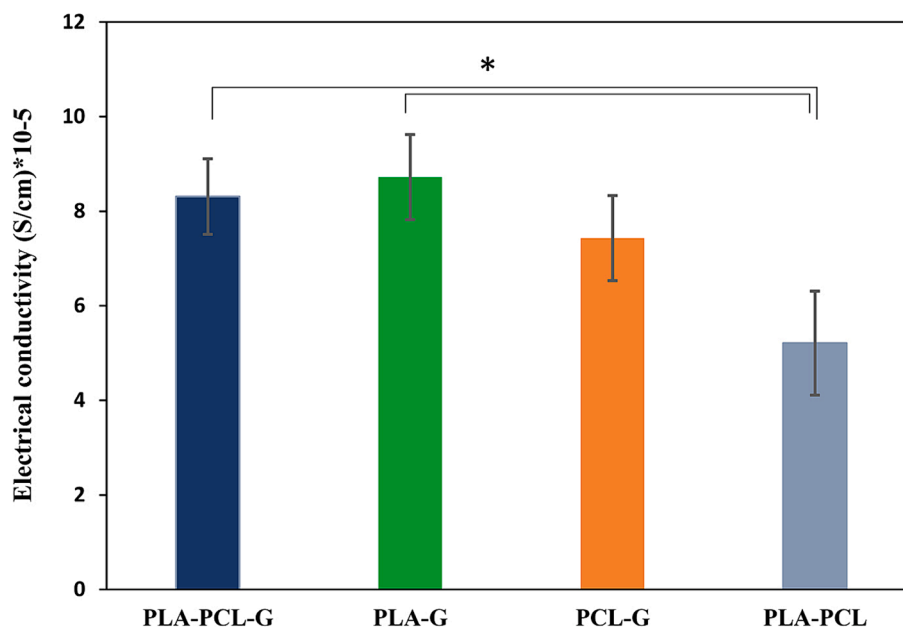


Fig. 7. The electrical conductivity of the scaffolds. a) PLA-PCL-G, b) PLA-G, c) PCL-G, and d) PLA-PCL scaffolds (\*  $P < 0.05$ ).

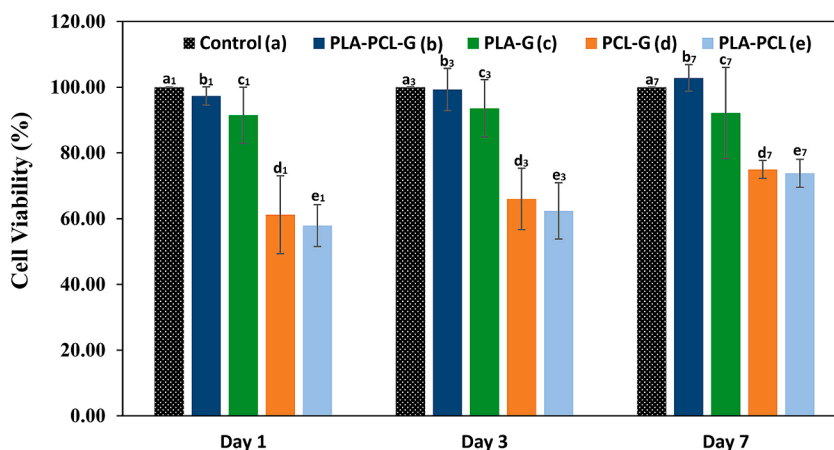
The specific characteristics of PLA, such as its ability to interact with graphene and form continuous networks, play a significant role in enhancing the overall conductivity of the composite materials (Stankovich et al., 2006; Kim et al., 2010; Lee et al., 2022; Moosa and Abed, 2021). If electrical conductivity is of interest, PLA-PCL-G and PLA-G samples can be suitable for this application.

The cytotoxicity of the scaffolds was evaluated at 1, 3, and 7 days (Fig. 8). On the first day, samples b1 and c1 showed significant cell survival and were non-toxic, whereas samples d1 and e1 exhibited poor cell survival, potentially due to their chemical composition. By the third day, none of the samples showed significant toxicity, with b3 and c3 samples demonstrating notable cell growth. However, by the seventh day, sample C7 displayed considerable fluctuation in cell viability and did not differ significantly from the other samples. Therefore, it cannot be considered an appropriate choice. Based on the cell viability data, PCL-PLA-G (b) appears to be a promising candidate for nerve tissue engineering.

SEM images in Fig. 9 depict PLA-PCL-G, PLA-G, PCL-G, and PCL-PLA samples after 3 days of cell culture. On the third day, all samples showed cell growth, but notably, the PLA-PCL-G sample (Fig. 9a) exhibited more pronounced cell growth. The scaffold was fully covered by a layer of cells, whereas the other samples did not exhibit complete cell coverage. The effective formulation and synergistic effect of PCL, PLA, and graphene are likely reasons for this cell layer formation, confirming the non-toxic nature of the scaffold. Based on the cytotoxicity and cell attachment results, the PLA-PCL-G scaffold is considered a suitable candidate for nerve tissue engineering.

#### 4. Conclusion

In this study, Poly(lactic acid)/poly( $\epsilon$ -caprolactone)/graphene (PLA/PCL/G) nanocomposite scaffolds were successfully fabricated using the fused deposition modeling (FDM) 3D printing method, aimed at peripheral nerve tissue engineering. The PLA-PCL-G scaffold, composed of



$P < 0.05$							
Day 1			Day 3			Day 7	
a <sub>1</sub> :d <sub>1</sub>	b <sub>1</sub> :d <sub>1</sub>	c <sub>1</sub> :d <sub>1</sub>	a <sub>3</sub> :d <sub>3</sub>	b <sub>3</sub> :d <sub>3</sub>	c <sub>3</sub> :d <sub>3</sub>	a <sub>7</sub> :d <sub>7</sub>	b <sub>7</sub> :d <sub>7</sub>
a <sub>1</sub> :e <sub>1</sub>	b <sub>1</sub> :e <sub>1</sub>	c <sub>1</sub> :e <sub>1</sub>	a <sub>3</sub> :e <sub>3</sub>	b <sub>3</sub> :e <sub>3</sub>	c <sub>3</sub> :e <sub>3</sub>	a <sub>7</sub> :e <sub>7</sub>	b <sub>7</sub> :e <sub>7</sub>

Fig. 8. MTT assay results of negative control, PLA-PCL-G, PLA-G, PCL-G, and PLA-PCL scaffolds.

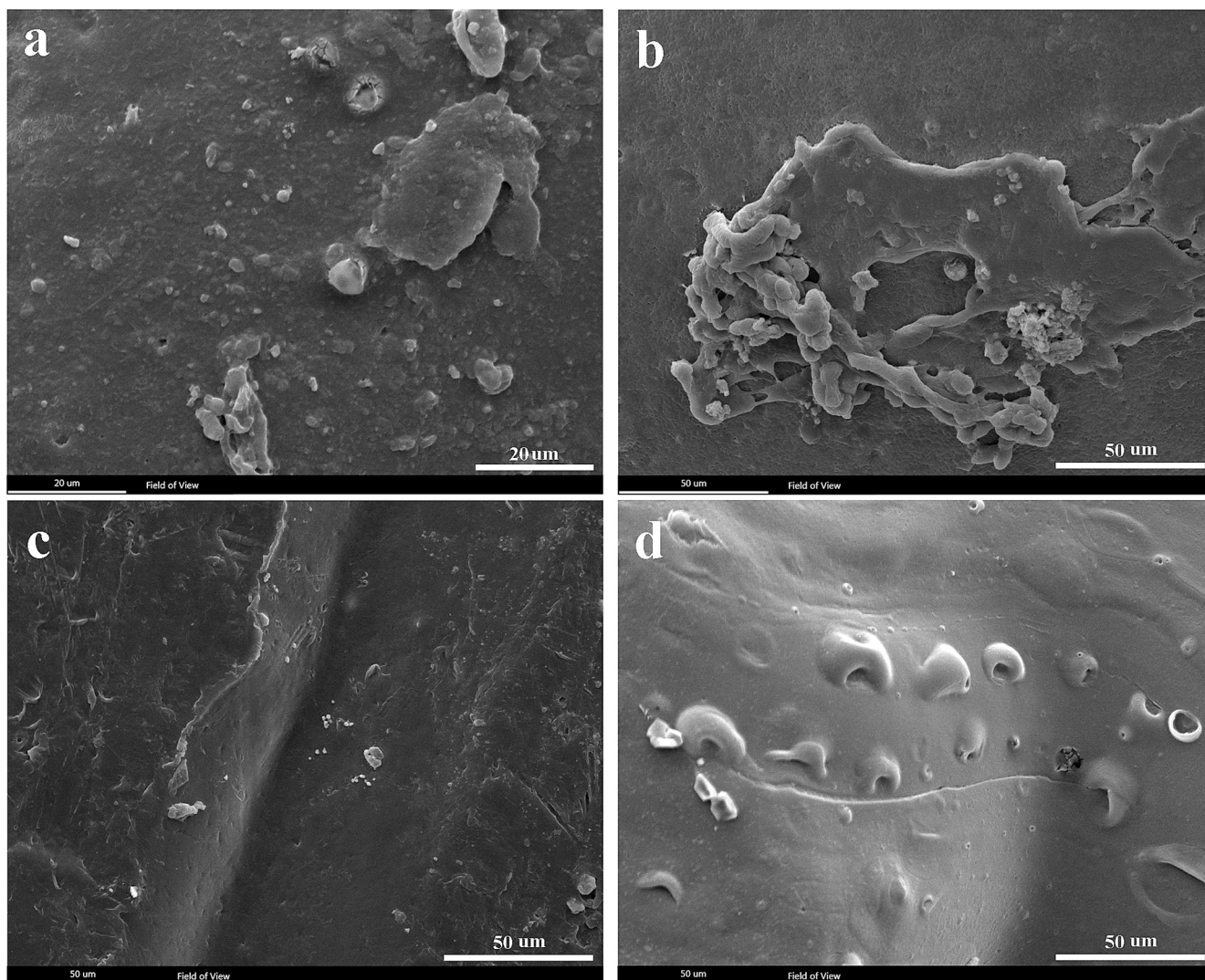


Fig. 9. SEM images of cell attachment on scaffolds after 3 days of cell culture. a) PLA-PCL-G, b) PLA-G, c) PCL-G, and d) PLA-PCL.

50 wt% PLA, 48.5 wt% PCL, and 1.5 wt% graphene, exhibited superior characteristics in terms of structural regularity, mechanical properties, electrical conductivity, and biocompatibility compared to other compositions tested. An elastic modulus of approximately 22.36 MPa and an electrical conductivity of  $8.2E-5$  S/cm were demonstrated by the scaffold, making it suitable for nerve tissue applications. The biodegradability study indicated a weight loss of 1.3 % and a degradation rate of 0.14 mm/day over four weeks, aligning well with peripheral nerve tissue regeneration rates. Additionally, the non-cytotoxic nature of the PLA-PCL-G scaffold to PC12 cells was confirmed by the MTT assay, underscoring its potential as a promising material for peripheral nerve tissue engineering.

#### CRediT authorship contribution statement

**Reyhane Soltani Gerdefaramarzi:** Writing – original draft, Methodology, Investigation, Formal analysis. **Mehdi Ebrahimian-Hosseini-nabadi:** Writing – review & editing, Supervision, Resources, Project administration, Methodology, Conceptualization. **Mohammad Khodaei:** Writing – review & editing, Supervision, Resources, Project administration, Methodology, Conceptualization.

#### Declaration of competing interest

The authors declare that they have no known competing financial interests or personal relationships that could have appeared to influence the work reported in this paper.

#### Acknowledgments

The authors acknowledge the support of the University of Isfahan (UI) in IRAN.

#### Prime Novelty Statement

The prime novelty of this research lies in the development of a PLA/PCL/graphene nanocomposite scaffold using FDM 3D printing, which combines the advantageous properties of PLA, PCL, and graphene. This novel scaffold not only enhances the structural and mechanical properties

#### References

- An, J., Teoh, J.E.M., Suntornnond, R., Chua, C.K., 2015. Design and 3D printing of scaffolds and tissues. *Engineering* 1 (2), 261–268. <https://doi.org/10.15302/J-ENG-2015061>.

- Bayer, I.S., 2017. Thermomechanical properties of polylactic acid-graphene composites: a state-of-the-art review for biomedical applications. *Materials* 10 (7), 748. <https://doi.org/10.3390/ma10070748>.
- Bei, H.P., Yang, Y., Zhang, Q., Tian, Y., Luo, X., Yang, M., Zhao, X., 2019. Graphene-based nanocomposites for neural tissue engineering. *Molecules* 24 (4), 658. <https://doi.org/10.3390/molecules24040658>.
- Bhandari, P.S., 2019. Management of peripheral nerve injury. *J. Clin. Orthopaed. Trauma* 10 (5), 862–866. <https://doi.org/10.1016/j.jcot.2019.08.003>.
- Ceretti, E., Ginestra, P., Neto, P.L., Fiorentino, A., Da Silva, J.V.L., 2017. Multi-layered scaffolds production via fused deposition modeling (FDM) using an open source 3D printer: process parameters optimization for dimensional accuracy and design reproducibility. *Procedia Cirp* 65, 13–18. <https://doi.org/10.1016/j.procir.2017.04.042>.
- Chiesa, E., Dorati, R., Pisani, S., Bruni, G., Rizzi, L.G., Conti, B., Genta, I., 2020. Graphene nanoplatelets for the development of reinforced PLA-PCL electrospun fibers as the next-generation of biomedical mats. *Polymers* 12 (6), 1390. <https://doi.org/10.3390/polym12061390>.
- Costa, L.S., Aidar, F.J., Matos, D.G.D., Oliveira, J.U.D., Santos, J.L.D., Almeida-Neto, P.F.D., Teixeira, M.M., 2020. Effects of resistance training and bowditchia virgilioides hydroethanolic extract on oxidative stress markers in rats submitted to peripheral nerve injury. *Antioxidants* 9 (10), 941. <https://doi.org/10.3390/antiox9100941>.
- Ebrahimian-Hosseiniabadi, M., Ashrafzadeh, F., Etemadifar, M., Venkatraman, S.S., 2011. Evaluating and modeling the mechanical properties of the prepared PLGA/nano-BCP composite scaffolds for bone tissue engineering. *J. Mater. Sci. Technol.* 27 (12), 1105–1112. [https://doi.org/10.1016/S1005-0302\(12\)60004-8](https://doi.org/10.1016/S1005-0302(12)60004-8).
- Eshraghi, S., Das, S., 2010. Mechanical and microstructural properties of polycaprolactone scaffolds with 1-D, 2-D, and 3-D orthogonally oriented porous architectures produced by selective laser sintering. *Acta Biomater.* 6 (7), 2467. <https://doi.org/10.1016/j.actbio.2010.02.002>.
- Firoozabadi, F.D., Saadatnabadi, A.R., Asefnejad, A., 2022. Fabrication and evaluation of in vitro studies of biodegradable and antibacterial composite scaffolds based on polylactic acid-polycaprolactone-hydroxyapatite reinforced with graphene and zinc oxide nanoparticles for use in orthopedic surgery. *Iran. J. Mater. Sci. Eng.* 19, 1–19. <https://doi.org/10.22068/ijmse.2788>.
- Fornasari, B.E., Carta, G., Gambarotta, G., Raimondo, S., 2020. Natural-based biomaterials for peripheral nerve injury repair. *Front. Bioeng. Biotechnol.* 8, 554257. <https://doi.org/10.3389/fbioe.2020.554257>.
- Foroutan, S., Hashemian, M., Khosravi, M., Nejad, M.G., Asefnejad, A., Saber-Samandari, S., Khandan, A., 2021. A porous sodium alginate-CaSiO<sub>3</sub> polymer reinforced with graphene nanosheet: fabrication and optimality analysis. *Fibers Polym.* 22, 540–549. <https://doi.org/10.1007/s12221-021-0347-9>.
- Fu, X., Zhu, Y., Li, J., Jiang, L., Zhao, X., Fan, X., 2021. Preparation, characterization and application of nano-graphene-based energetic materials. *Nanomaterials* 11 (9), 2374. <https://doi.org/10.3390/nano11092374>.
- Geetha Bai, R., Muthoosamy, K., Manickam, S., Hilal-Alnaqbi, A., 2019. Graphene-based 3D scaffolds in tissue engineering: fabrication, applications, and future scope in liver tissue engineering. *Int. J. Nanomed.* 5753–5783. <https://doi.org/10.2147/IJN.S192779>.
- Hasheminejad, K., Montazeri, A., 2020. Enhanced interfacial characteristics in PLA/graphene composites through numerically-designed interface treatment. *Appl. Surf. Sci.* 502, 144150. <https://doi.org/10.1016/j.apsusc.2019.144150>.
- Howarth, H.M., Alaziz, T., Nicolds, B., O'Connor, S., Shah, S.B., 2019. Redistribution of nerve strain enables end-to-end repair under tension without inhibiting nerve regeneration. *Neural Regen. Res.* 14 (7), 1280–1288. <https://doi.org/10.4103/1673-5374.251338>.
- Iranmanesh, P., Ehsani, A., Khademi, A., Asefnejad, A., Shahriari, S., Soleimani, M., Khandan, A., 2022. Application of 3D bioprinters for dental pulp regeneration and tissue engineering (porous architecture). *Transp. Porous Media* 142 (1), 265–293. <https://doi.org/10.1007/s11242-021-01618-x>.
- JAWEED, M., 1994. *Peripheral nerve regeneration*. In: *The Physiological Basis of Rehabilitation Medicine* (pp. 543–561). Butterworth-Heinemann. DOI: 10.1016/B978-1-4831-7818-9.50027-7.
- Kamble, N., Shukla, D., Bhat, D., 2019. Peripheral nerve injuries: electrophysiology for the neurosurgeon. *Neurol. India* 67 (6), 1419–1422. <https://doi.org/10.4103/0028-3886.273626>.
- Kamiloglu Bestepe, S.E.N.E.M., Sari, G., Özdal, T., Çapanoğlu Güven, E., 2020. Guidelines for cell viability assays. *Food Front.* 1 (3). <https://doi.org/10.1002/fft.2.44>.
- Karimi, M., Asefnejad, A., Aflaki, D., Surendar, A., Baharifar, H., Saber-Samandari, S., Toghraie, D., 2021. Fabrication of shapeless scaffolds reinforced with baghdadite-magnetite nanoparticles using a 3D printer and freeze-drying technique. *J. Mater. Res. Technol.* 14, 3070–3079. <https://doi.org/10.1016/j.jmrt.2021.08.084>.
- Kasmi, S., Cayuela, J., Backer, B.D., Labbé, E., Alix, S., 2021. Modified polylactic acid with improved impact resistance in the presence of a thermoplastic elastomer and the influence of fused filament fabrication on its physical properties. *J. Compos. Sci.* 5 (9), 232. <https://doi.org/10.3390/jcs5090232>.
- Khajehmohammadi, M., Azizi Tafti, R., Nikukar, H., 2023. Effect of porosity on mechanical and biological properties of bioprinted scaffolds. *J. Biomed. Mater. Res.* A 111 (2), 245–260. <https://doi.org/10.1002/jbm.a.37455>.
- Kim, H., Abdala, A.A., Macosko, C.W., 2010. Graphene/polymer nanocomposites. *Macromolecules* 43 (16), 6515–6530. <https://doi.org/10.1021/ma100572e>.
- Kim, M., Jeong, J.H., Lee, J.Y., Capasso, A., Bonaccorso, F., Kang, S.H., Lee, G.H., 2019. Electrically conducting and mechanically strong graphene-poly(lactic acid) composites for 3D printing. *ACS Appl. Mater. Interfaces* 11 (12), 11841–11848. <https://doi.org/10.1021/acsami.9b03241>.
- Kumar, P., Dehiya, B.S., Sindhu, A., 2017. Comparative study of chitosan and chitosan-gelatin scaffold for tissue engineering. *Int. Nano Lett.* 7, 285–290. <https://doi.org/10.1007/s40089-017-0222-2>.
- Lee, S.J., Yoo, J.J., Atala, A., 2018. Biomaterials and tissue engineering. *Clin. Regenerat. Med. Urol.* 17–51. [https://doi.org/10.1007/978-981-10-2723-9\\_2](https://doi.org/10.1007/978-981-10-2723-9_2).
- Lee, S.J., Yoon, S.J., Jeon, I.Y., 2022. Graphene/polymer nanocomposites: preparation, mechanical properties, and application. *Polymers* 14 (21), 4733. <https://doi.org/10.3390/polym14214733>.
- Lei, M., Wei, Q., Li, M., Zhang, J., Yang, R., Wang, Y., 2022. Numerical simulation and experimental study the effects of process parameters on filament morphology and mechanical properties of FDM 3D printed PLA/GNPs nanocomposite. *Polymers* 14 (15), 3081. <https://doi.org/10.3390/polym14153081>.
- Lopes, B., Sousa, P., Alvites, R., Branquinho, M., Sousa, A.C., Mendonça, C., Maurício, A. C., 2022. Peripheral nerve injury treatments and advances: one health perspective. *Int. J. Mol. Sci.* 23 (2), 918. <https://doi.org/10.3390/ijms23020918>.
- Magaz, A., Faroni, A., Gough, J.E., Reid, A.J., Li, X., Blaker, J.J., 2018. Bioactive silk-based nerve guidance conduits for augmenting peripheral nerve repair. *Adv. Healthc. Mater.* 7 (23), 1800308. <https://doi.org/10.1002/adhm.201800308>.
- Mankavi, F., Ibrahim, R., Wang, H., 2023. Advances in biomimetic nerve guidance conduits for peripheral nerve regeneration. *Nanomaterials* 13 (18), 2528. <https://doi.org/10.3390/nano13182528>.
- Masarra, N.A., Batistella, M., Quantin, J.C., Regazzi, A., Pucci, M.F., El Hage, R., Lopez-Cuesta, J.M., 2022. Fabrication of PLA/PCL/graphene nanoplatelet (GNP) electrically conductive circuit using the fused filament fabrication (FFF) 3D printing technique. *Materials* 15 (3), 762. <https://doi.org/10.3390/ma15030762>.
- Masood, S.H., 2014. Advances in fused deposition modeling. *Compreh. Mater. Process.* 10, 69–91. <https://doi.org/10.1016/B978-0-08-096532-1.01002-5>.
- Moosa, A., Abed, M., 2021. Graphene preparation and graphite exfoliation. *Turk. J. Chem.* 45 (3), 493–519. <https://doi.org/10.3906/kim-2101-19>.
- Naghieh, S., Ravari, M.K., Badrossamay, M., Foroozmehr, E., Kadkhodaei, M., 2016. Numerical investigation of the mechanical properties of the additive manufactured bone scaffolds fabricated by FDM: the effect of layer penetration and post-heating. *J. Mech. Behav. Biomed. Mater.* 59, 241–250. <https://doi.org/10.1016/j.jmbm.2016.01.031>.
- Novoselov, K.S., Colombo, L., Gellert, P.R., Schwab, M.G., Kim, K.A.J.N., 2012. A roadmap for graphene. *Nature* 490 (7419), 192–200. <https://doi.org/10.1038/nature11458>.
- Papageorgiou, D.G., Kinloch, I.A., Young, R.J., 2017. Mechanical properties of graphene and graphene-based nanocomposites. *Prog. Mater. Sci.* 90, 75–127. <https://doi.org/10.1016/j.pmatsci.2017.07.004>.
- Park, J., Jeon, J., Kim, B., Lee, M.S., Park, S., Lim, J., Lee, J.Y., 2020. Electrically conductive hydrogel nerve guidance conduits for peripheral nerve regeneration. *Adv. Funct. Mater.* 30 (39), 2003759. <https://doi.org/10.1002/adfm.202003759>.
- Pedrosa, S.S., Caseiro, A.R., Santos, J.D., Maurício, A.C., 2017. Scaffolds for peripheral nerve regeneration, the importance of in vitro and in vivo studies for the development of cell-based therapies and biomaterials: state of the art. *Scaffolds Tissue Eng. Mater. Technol. Clin. Appl.* 9 (12), 179. <https://doi.org/10.5772/intechopen.69540>.
- Ramazani, S., Karimi, M., 2016. Study the molecular structure of poly ( $\epsilon$ -caprolactone)/graphene oxide and graphene nanocomposite nanofibers. *J. Mech. Behav. Biomed. Mater.* 61, 484–492. <https://doi.org/10.1016/j.jmbm.2016.04.020>.
- Sazali, N., Ibrahim, H., Jamaludin, A. S., Mohamed, M. A., Salleh, W. N. W., Abidin, M.N. Z., 2020. Degradation and stability of polymer: a mini review. In: *IOP Conference Series: Materials Science and Engineering* (Vol. 788, No. 1, p. 012048). IOP Publishing. DOI: 10.1088/1757-899X/788/1/012048.
- Seddighi, A., Nikouei, A., Saied Seddighi, A., Reza Zali, A., Mahmood Tabatabaei, S., Reza Sheykhi, A., Naeimian, S., 2016. Peripheral nerve injury: a review article. *Int. Clin. Neurosci. J.* 3 (1), 1–6. <https://doi.org/10.22037/icnj.v3i1.12016>.
- Sensharma, P., Madhumathi, G., Jayant, R.D., Jaiswal, A.K., 2017. Biomaterials and cells for neural tissue engineering: current choices. *Mater. Sci. Eng. C* 77, 1302–1315. <https://doi.org/10.1016/j.msec.2017.03.264>.
- Seyedsalehi, A., Daneshmandi, L., Barajaa, M., Riordan, J., Laurencin, C.T., 2020. Fabrication and characterization of mechanically competent 3D printed polycaprolactone-reduced graphene oxide scaffolds. *Sci. Rep.* 10 (1), 22210. <https://doi.org/10.1038/s41598-020-78977-w>.
- Shamsah, A.H., Cartmell, S.H., Richardson, S.M., Bosworth, L.A., 2020. Material characterization of PCL: PLL electrospun fibers following six months degradation in vitro. *Polymers* 12 (3), 700. <https://doi.org/10.3390/polym12030700>.
- Stankovich, S., Dikin, D.A., Dommett, G.H., Kohlhaas, K.M., Zimney, E.J., Stach, E.A., et al., 2006. Graphene-based composite materials. *Nature* 442(7100), 282–286. DOI: 10.1038/nature04969.
- Sulaiman, W., Gordon, T., 2013. *Neurobiology of peripheral nerve injury, regeneration, and functional recovery: from bench top research to bedside application*. *Ochsner Journal* 13 (1), 100–108.
- Sun, P., Guan, Y., Yang, C., Hou, H., Liu, S., Yang, B., Yin, L., 2023. A bioresorbable and conductive scaffold integrating silicon membranes for peripheral nerve regeneration. *Adv. Healthc. Mater.* 12 (32), 2301859. <https://doi.org/10.1002/adhm.202301859>.
- Tian, J., Cao, Z., Qian, S., Xia, Y., Zhang, J., Kong, Y., Takahashi, J., 2022. Improving tensile strength and impact toughness of plasticized poly (lactic acid) biocomposites by incorporating nanofibrillated cellulose. *Nanotechnol. Rev.* 11 (1), 2469–2482. <https://doi.org/10.1515/ntrev-2022-0142>.
- Vaid, R., Yildirim, E., Pasquinelli, M.A., King, M.W., 2021. Hydrolytic degradation of polylactic acid fibers as a function of pH and exposure time. *Molecules* 26 (24), 7554. <https://doi.org/10.3390/molecules26247554>.
- Vijayavenkataraman, S., Kannan, S., Cao, T., Fuh, J.Y., Sriram, G., Lu, W.F., 2019. 3D-printed PCL/PPy conductive scaffolds as three-dimensional porous nerve guide

- conduits (NGCs) for peripheral nerve injury repair. *Front. Bioeng. Biotechnol.* 7, 266. <https://doi.org/10.3389/fbioe.2019.00266>.
- Wang, J., Liu, Y., Fan, Z., Wang, W., Wang, B., Guo, Z., 2019. Ink-based 3D printing technologies for graphene-based materials: a review. *Adv. Compos. Hybrid Mater.* 2, 1–33. <https://doi.org/10.1007/s42114-018-0067-9>.
- Wilcox, M., Gregory, H., Powell, R., Quick, T.J., Phillips, J.B., 2020. Strategies for peripheral nerve repair. *Curr. Tissue Microenviron. Rep.* 1, 49–59. <https://doi.org/10.1007/s43152-020-00002-z>.
- Wu, Y., An, C., Guo, Y., 2023. 3D printed graphene and graphene/polymer composites for multifunctional applications. *Materials* 16 (16), 5681. <https://doi.org/10.3390/ma16165681>.
- Wu, Y.S., Pruess, K., Persoff, P., 1998. Gas flow in porous media with Klinkenberg effects. *Transp. Porous Media* 32, 117–137. <https://doi.org/10.1023/A:1006535211684>.
- Yan, J., Wu, R., Liao, S., Jiang, M., Qian, Y., 2020. Applications of polydopamine-modified scaffolds in the peripheral nerve tissue engineering. *Front. Bioeng. Biotechnol.* 8, 590998 <https://doi.org/10.3389/fbioe.2020.590998>.
- Yen, C.M., Shen, C.C., Yang, Y.C., Liu, B.S., Lee, H.T., Sheu, M.L., Cheng, W.Y., 2019. Novel electrospun poly( $\epsilon$ -caprolactone)/type I collagen nanofiber conduits for repair of peripheral nerve injury. *Neural Regen. Res.* 14 (9), 1617. <https://doi.org/10.4103/1673-5374.255997>.
- Zakaria, H.M., 2014. Microstructural and corrosion behavior of Al/SiC metal matrix composites. *Ain Shams Eng. J.* 5 (3), 831–838. <https://doi.org/10.1016/j.asej.2014.03.003>.
- Zhang, P.X., Han, N., Kou, Y.H., Zhu, Q.T., Liu, X.L., Quan, D.P., Jiang, B.G., 2019. Tissue engineering for the repair of peripheral nerve injury. *Neural Regen. Res.* 14 (1), 51–58. <https://doi.org/10.4103/1673-5374.243701>.
- Zhang, Y., Wang, S., Yang, P., 2020. Effects of graphene-based materials on the behavior of neural stem cells. *J. Nanomater.* 2020 (1), 2519105. <https://doi.org/10.1155/2020/2519105>.
- Zhang, Y., Sun, N., Zhu, M., Qiu, Q., Zhao, P., Zheng, C., Lu, T., 2022. The contribution of pore size and porosity of 3D printed porous titanium scaffolds to osteogenesis. *Biomater. Adv.* 133, 112651 <https://doi.org/10.1016/j.msec.2022.112651>.